



**HAL**  
open science

# $\pi$ -Extended Porphyrin–Phthalocyanine Heterojunction Devices Exhibiting High Ammonia Sensitivity with a Remarkable Light Effect

Sujithkumar Ganesh Moorthy, Jacob Arvidson, Rita Meunier-Prest, Hong Wang, Marcel Bouvet

► **To cite this version:**

Sujithkumar Ganesh Moorthy, Jacob Arvidson, Rita Meunier-Prest, Hong Wang, Marcel Bouvet.  $\pi$ -Extended Porphyrin–Phthalocyanine Heterojunction Devices Exhibiting High Ammonia Sensitivity with a Remarkable Light Effect. *ACS Sensors*, 2024, 9 (2), pp.883-894. 10.1021/acssensors.3c02247 . hal-04612610

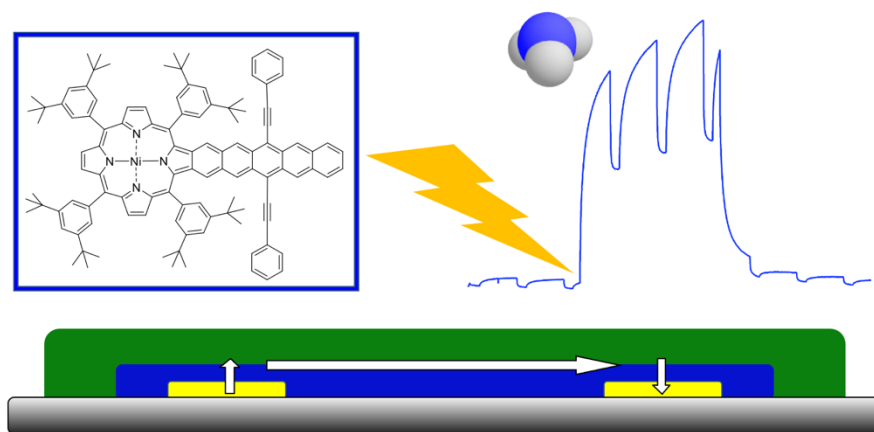
**HAL Id: hal-04612610**

**<https://hal.science/hal-04612610v1>**

Submitted on 14 Jun 2024

**HAL** is a multi-disciplinary open access archive for the deposit and dissemination of scientific research documents, whether they are published or not. The documents may come from teaching and research institutions in France or abroad, or from public or private research centers.

L'archive ouverte pluridisciplinaire **HAL**, est destinée au dépôt et à la diffusion de documents scientifiques de niveau recherche, publiés ou non, émanant des établissements d'enseignement et de recherche français ou étrangers, des laboratoires publics ou privés.



## **$\pi$ -Extended porphyrin-phthalocyanine heterojunction devices exhibiting high ammonia sensitivity with a remarkable light effect**

Sujithkumar Ganesh Moorthy,<sup>a</sup> Jacob Arvidson<sup>b</sup>, Rita Meunier-Prest,<sup>a</sup> Hong Wang<sup>b\*</sup>, Marcel Bouvet,<sup>a\*</sup>

<sup>a</sup>Institut de Chimie Moléculaire de l'Université de Bourgogne (ICMUB), UMR CNRS 6302, Université de Bourgogne, 9 avenue Alain Savary, 21078 Dijon cedex, France. Fax: +33-380-396-098; Tel : +33-380-396-086; E-mail: marcel.bouvet@u-bourgogne.fr

<sup>b</sup>Department of Chemistry, University of North Texas, 1508 W. Mulberry St, Denton, TX, USA, 76203; E-mail: hong.wang@unt.edu

### **Abstract**

$\pi$ -Extended porphyrins represent an attractive class of organic compounds because of their unique photophysical, optoelectronic and physicochemical properties. Herein, a cross-conjugated (Ace-PQ-Ni) and a linear-conjugated (AM6) porphyrins are used to build double layer heterojunction devices by combining with lutetium bisphthalocyanine complex (LuPc<sub>2</sub>). The heterojunction effect at the porphyrin-phthalocyanine interface plays a key role in their charge transport properties. Both devices exhibit exceptionally high ammonia sensitivity at room temperature and under ambient relative humidity, with a limit of detection as good as 156 and 115 ppb for Ace-PQ-Ni/LuPc<sub>2</sub> and AM6/LuPc<sub>2</sub> sensors, respectively. Interestingly, Ace-PQ-Ni/LuPc<sub>2</sub> and AM6/LuPc<sub>2</sub> sensors display opposite effect upon light illumination. While the former show largely decreased ammonia sensitivity under light illumination, the current variation of the latter under ammonia is remarkably enhanced with multiplication factor of 13 and a LOD as good as 83 ppb. Their strikingly difference in sensing properties upon light illumination is attributed to their different  $\pi$ -conjugation pathways (cross-conjugation versus linear-conjugation).

**Keywords:** Molecular materials;  $\pi$ -Extended porphyrin; Linear conjugation; Cross conjugation; Molecular semiconductor; Conductometric transducer; Heterojunction; Relative humidity

Porphyrins known as pigments of life offer a wide range of interaction mechanisms for analyte binding, mainly through Van der Waals interactions,  $\pi$ - $\pi$  interactions and coordination to the central metal ion. The richness of their properties has been taken advantage of to develop gas sensors, associated mainly to optical<sup>1,2</sup> and acoustic<sup>3,4</sup> transducers. Due to their rather poor conducting properties, porphyrins have been rarely used directly as sensing materials in conductometric sensors<sup>5</sup>. However, they were more studied for carbonaceous materials, such as carbon nanotubes<sup>6-8</sup>. Recently, we introduced polyporphyrins in two types of gas sensing heterostructures (Fig. 1) including double lateral heterojunctions<sup>9</sup> and double layer heterojunctions<sup>10</sup>. In double lateral heterojunctions<sup>9</sup>, polyporphyrins were electrodeposited on interdigitated electrodes, then covered by a molecular semiconductor, i.e. lutetium bisphthalocyanine LuPc<sub>2</sub>. In double layer heterojunctions<sup>10</sup>, polyporphyrins were synthesized and deposited by chemical vapor deposition technique, in the presence of an oxidizing species, on a poor conducting phthalocyanine material. In the former devices, electrosynthesis of zinc porphine – a non-substituted porphyrin – at low positive potential, to obtain a low conjugated and poor conducting polymer, allowing for the heterojunction effect to play a key role. In the latter case, polyporphyrins obtained from nickel tetraphenyl and nickel tetramesityl porphyrins were highly conjugated, leading to another type of heterojunction effect<sup>11,12</sup>.

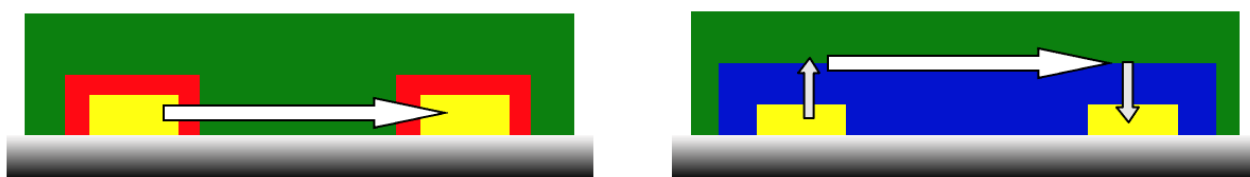


**Figure 1.** Scheme of a double lateral heterojunction (left) and a double layer heterojunction (right).

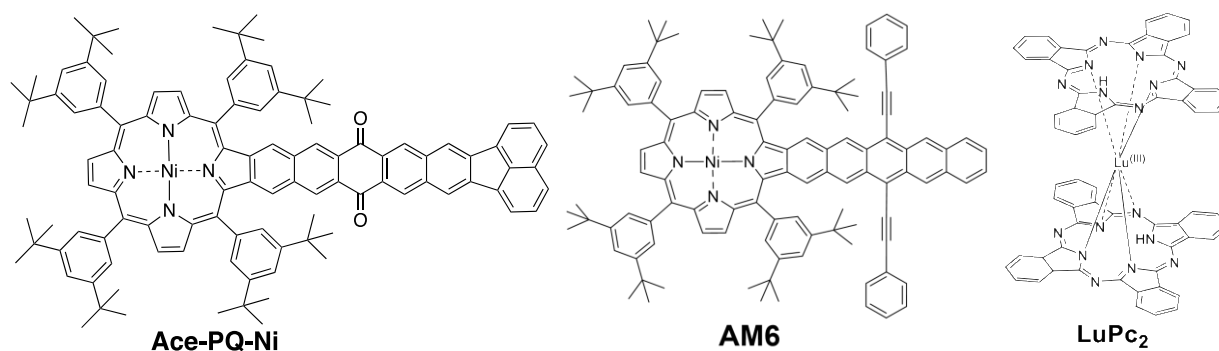
Semiconductors based on metal oxides have been often used as active materials in gas sensors. It is well-known that photoexcitation can affect transport phenomena by increasing the

density of free charge carriers and by decreasing the energy barrier at grain boundaries<sup>13</sup>. Thus, illumination can also change trapping phenomena by changing the occupancy of defects by electrons and holes. In terms of gas sensing, relative response can be increased and response time can be shortened under light. It has been reported that the response was multiplied by ca. 6<sup>13</sup> upon UV irradiation on SnO<sub>2</sub> exposed to CO (100 ppm, RT) or NO<sub>2</sub> (1 ppm, 300°C). With In<sub>2</sub>O<sub>3</sub>, RR was multiplied by 16 at 100 ppm CO, while RR was quasi unchanged at 3 ppm NO<sub>2</sub>, but with a better recovery and improved kinetics at RT. To explain these observations, the authors hypothesized that light helps oxygen desorption, and consequently facilitates CO adsorption. However, response can also decrease depending on light energy, even though recovery time is shortened<sup>14</sup>, suggesting complex light effect. Improved response time by a factor of ten was reported by Llobet et al. for pulsed UV light illuminated on WO<sub>3</sub> nanoneedles exposed to NO<sub>2</sub> or NH<sub>3</sub><sup>15</sup>. Nakamura and co-workers reported an interesting *p*-NiO/*n*-ZnO heterojunction, for which sensing performances for aromatic volatile organic compounds (VOCs) were highly improved under deep UV light irradiation, as a result of an electron transfer from the photo-excited VOC adsorbates to the valence band (VB) of *p*-NiO<sup>16</sup>. A high sensitivity increase was also observed with visible light on inorganic halide perovskites used to detect O<sub>2</sub>, and volatile small organic molecules including acetone and ethyl alcohol<sup>17</sup>. Di Natale et al. reported the use of visible light effect to tune the selectivity of porphyrin coated ZnO hybrid material towards VOCs<sup>18,19</sup>. In this case, light induces not only a photocurrent as in any junction-based solar cell, but also promotes the selectivity towards amines compared to alcohols. Obviously, mechanisms involved in metal oxide – based resistors or heterojunctions cannot be directly applied to molecular material – based sensors. Actually, only a few examples of light effect on molecular material-based gas sensors were reported. An increase in sensitivity towards water, ethyl alcohol and dimethyl methyl phosphonate (DMMP) was reported for graphene field-effect transistor under UV light<sup>20</sup>. Using copper octafluoro-phthalocyanine/LuPc<sub>2</sub> heterojunction devices, we have also demonstrated that visible

light from red LEDs was capable to inverse the polarity of majority free charge carriers from p- to n-type, as a result of oxygen desorption, which acts as a trap for negative charges<sup>21</sup>.

LuPc<sub>2</sub> is known as the first intrinsic semiconductor<sup>22,23</sup>. Its unique behavior is due to its radical nature, which allows an easy electron transfer from or towards LuPc<sub>2</sub> neighboring molecules. Thus, activation energy of its dark conductivity is very low, ca. 0.5 eV, against more than 1 eV for all other molecular materials, which are less conductive. In the present heterojunctions, the high conductivity of LuPc<sub>2</sub> compared to the sub-layers imposes charges to flow from one electrode to the other one through the interface, as shown in Fig. 1 right<sup>24</sup>. To understand such heterojunction devices, we need to keep in mind the behavior of molecular material-based heterojunction devices, in particular the formation of a conducting channel by charge accumulation at the interface between both layers<sup>11</sup>. This is very different from what happens in inorganic heterojunctions in which a depleted zone is formed.

In this work, we report the use of two original highly  $\pi$ -conjugated porphyrin complexes in double layer heterojunction devices, in combination with LuPc<sub>2</sub> as a top layer and their response to ammonia.  $\pi$ -Extended porphyrins have received particular attention due to their unique photophysical and optoelectronic properties<sup>25,26</sup>. Recently, one of us (Wang) reported the synthesis of unsymmetric polycyclic aromatic hydrocarbon (PAH) – fused porphyrins, i.e. pentacenequinone – fused (cross-conjugated) and pentacene – fused porphyrins (linear-conjugated)<sup>27</sup>, which can potentially lead to original electrical properties. Despite their similar D<sub>2h</sub> symmetry, they display very different optical and electronic properties, due to the type of conjugation involved. In the former, conjugation is extended on all the pentacene moiety, while in the later the quinone carbonyl fragment interrupts the  $\pi$ -conjugation. Precisely, the porphyrin complexes reported in this work are pentacene-fused nickel porphyrin (AM6) and acenaphtho[1,2-b]pentacene-9,16-dione-fused nickel porphyrins (Ace-PQ-Ni) (Scheme 1). We also studied the effect of illumination on electrical and sensing responses.



**Scheme 1.** Chemical structure of acenaphtho[1,2-b]pentacene-9,16-dione-fused nickel porphyrin (Ace-PQ-Ni), pentacene-fused nickel porphyrin (AM6), and lutetium bisphthalocyanine (LuPc<sub>2</sub>) (from left to right).

## Experimental section

### Chemicals

The synthesis - starting from 1,2-dibromoacenaphthylene, purification and characterization of acenaphtho[1,2-b]pentacene-9,16-dione-fused nickel porphyrin (C<sub>106</sub>H<sub>104</sub>N<sub>4</sub>NiO<sub>2</sub>) (Ace-PQ-Ni) are described in the Supporting Information. <sup>1</sup>H and <sup>13</sup>C NMR spectra are given in Figures S1 to S6. Monoporphyrin-fused pentacene (C<sub>112</sub>H<sub>112</sub>N<sub>4</sub>Ni) (AM6)<sup>27-29</sup> and lutetium bisphthalocyanine (LuPc<sub>2</sub>)<sup>30</sup> were synthesized and purified according to published procedures.

### Sensors development and electrical measurements

Organic heterojunction sensors were fabricated by depositing Ace-PQ-Ni and AM6 as sublayers and lutetium bisphthalocyanine (LuPc<sub>2</sub>) as a top layer on Indium Tin Oxide (ITO) interdigitated electrodes (IDEs) lithographically patterned on glass substrates. The IDE consisted of 125 pairs of ITO digits, having a width and spacing between two digits as 10 μm. Electrodes were properly cleaned through stepwise ultrasonication in CH<sub>2</sub>Cl<sub>2</sub> and ethanol followed by drying in an oven for 1 hr at 100°C. The sublayers were coated on IDE by using quasi dip coating method that we developed recently<sup>31</sup> (Scheme S1) and bilayer heterostructures were fabricated on the Ace-PQ-Ni and AM6 resistors by thermal evaporation in UNIVEX 250 thermal evaporator under

secondary vacuum (ca.  $10^{-7}$  mbar). 50 nm-thick layer of LuPc<sub>2</sub> was deposited on the sublayer at a rate of ca.  $0.7 \text{ \AA s}^{-1}$ . The sublimation temperature for LuPc<sub>2</sub> was noted in the range 400 – 450°C. Current-Voltage (I-V) characterization and sensing measurements of the heterojunction sensors were performed at room temperature (18 – 21°C) using a Keithley 6517B electrometer, at bias ranging from -10 V to +10 V in steps of 0.1 V. Impedance spectroscopy measurements were performed on a Solartron SI 1260 impedance analyser. The interface of the bilayer heterojunctions was studied over a wide range of frequencies (from 10 Hz to 10 MHz) with fixed AC (200 mV) and varying DC bias from 0 to 10 V. Obtained data were treated using Ametek's Zview software. Electrical properties were also obtained under UV light using EvoluChem 365 nm UV light source (HCK1012-01-011).

### **Characterization techniques**

Electronic absorption spectra of different porphyrins, LuPc<sub>2</sub> and the bilayer films were registered using a Cary 50 (Varian) UV-vis spectrophotometer, between 300 nm and 850 nm. Raman spectral measurement of different films and materials was conducted using Renishaw inVia Raman microscope, utilizing 473 nm laser as an excitation source.

### **Gas sources and sensing experiments**

Ammonia gas, at 985 ppm and 98 ppm (mol/mol) in synthetic air and synthetic air were used from standard commercial cylinders, purchased from Air Liquide, France. A water column was used to generate humidity saturated synthetic air. Then, the RH value was measured, after dilution by dry synthetic air, by a humidity sensor (HMT 100, Vaisala, Finland). A small flow of NH<sub>3</sub> (ca. 5 to 50 NmL min<sup>-1</sup>) was added to the previous flow to generate air with controlled NH<sub>3</sub> concentrations, in the range 10-90 ppm or 1-9 ppm, depending on the concentration in the NH<sub>3</sub>/air cylinders. The total flow was kept constant in all experiments, namely 550 NmL min<sup>-1</sup>. The RH values given in the text are those calculated in the final flow sent through the test cell (volume: 8 cm<sup>3</sup>). Gas flow in different fluidic lines was controlled by mass flow controllers and electronic

valves, which were interfaced with a homemade software. The scheme of the setup used for electrical and sensing measurements was the same as in our previous work<sup>21,32</sup>.

## **Results and Discussion**

### **Optical characterizations of bilayer heterostructures**

The normalized optical absorption spectra of each layer as well as the resulting bilayer heterostructures were displayed in Figure 2a and 2b. Both bilayer films exhibit typical porphyrin absorption peaks from sublayer that correspond to Soret band region spanning at 428, 460, 493 and 577 nm in Ace-PQ-Ni/LuPc<sub>2</sub> and at 435 nm in AM6/LuPc<sub>2</sub><sup>1</sup>. Several weaker bands of AM6 between 600 to 704 nm were overlapped with a main peak of LuPc<sub>2</sub> at 669 nm. In both bilayer films, most of the peaks from sublayer were overlapped with the peaks from top layer resulting in change in peak intensity, e.g. the peak at 459 nm (strong in Ace-PQ-Ni) was overlapped with peak at 468 nm (weak in LuPc<sub>2</sub>) and appears at 462 nm (medium in Ace-PQ-Ni/LuPc<sub>2</sub> heterostructure). This peak in LuPc<sub>2</sub> that appears as a shoulder at 470 nm in AM6/LuPc<sub>2</sub> bilayer films corresponds to the transition between a filled orbital towards the semi occupied molecular orbital (SOMO) of LuPc<sub>2</sub><sup>33,34</sup>.

Raman spectroscopy measurements were performed on powders of Ace-PQ-Ni, AM6, LuPc<sub>2</sub> and their corresponding bilayer heterostructures. The Raman spectra of the bilayer clearly show a combination of peaks that correspond to the chemical fingerprints of the LuPc<sub>2</sub> layer and the Ace-PQ-Ni or AM6 layer (Fig. 2c and 2d). The sublayer of both heterojunction devices are highly Raman active compared to top layer. In Ace-PQ-Ni/LuPc<sub>2</sub> heterostructure, the medium intense peaks at 1270 cm<sup>-1</sup>, 1352 cm<sup>-1</sup>, 1381 cm<sup>-1</sup>, 1429 cm<sup>-1</sup>, 1568 cm<sup>-1</sup>, 1589 cm<sup>-1</sup>, and the strong intense peaks at 1140 cm<sup>-1</sup> and 1658 cm<sup>-1</sup> particularly belong to the sublayer (Ace-PQ-Ni). In AM6/LuPc<sub>2</sub> heterostructure, peaks at 772 cm<sup>-1</sup>, 831 cm<sup>-1</sup>, 1075 cm<sup>-1</sup>, 1287 cm<sup>-1</sup>, 1372 cm<sup>-1</sup>, 1656 cm<sup>-1</sup> and the strongest peak at 1565 cm<sup>-1</sup> belong to AM6. The results were compiled in Table S1.

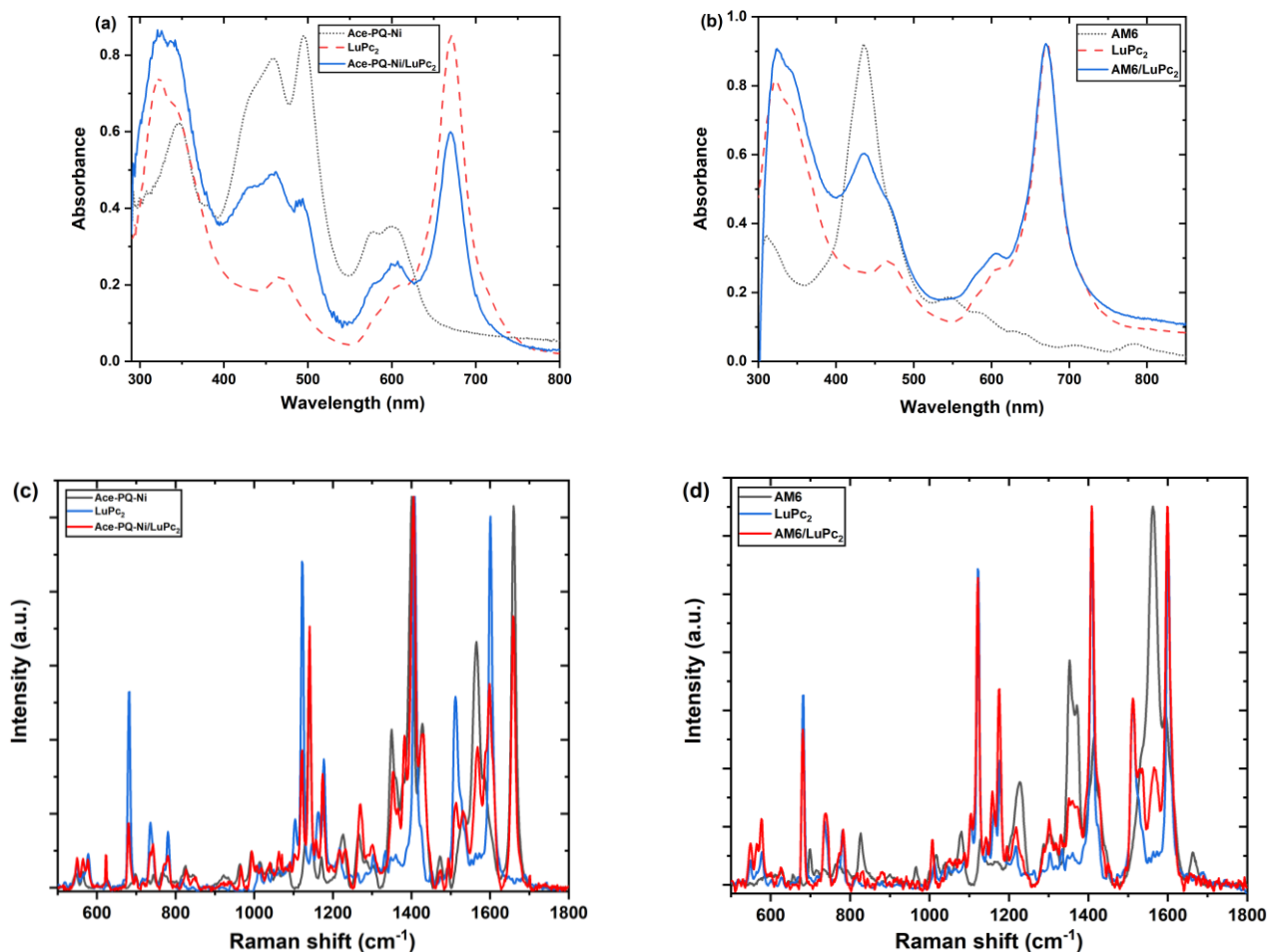


**Figure 2.** Comparison of normalized UV-vis spectra of (a) a Ace-PQ-Ni/LuPc<sub>2</sub> bilayer (blue line) with individual layers of LuPc<sub>2</sub> (red, dashed line) and Ace-PQ-Ni (black, dotted line) and (b) a AM6/LuPc<sub>2</sub> bilayer (blue line), AM6 (black, dotted line), and LuPc<sub>2</sub> (red, dashed line), and superimposition of the Raman spectra of Ace-PQ-Ni/LuPc<sub>2</sub> (c) and AM6/LuPc<sub>2</sub> (d) bilayers with the respective spectra of their constituents.

Most of the peaks from LuPc<sub>2</sub> overlap with peaks from sublayer, resulting in change in peak intensity, e.g. the peak at 682 cm<sup>-1</sup> (strong in LuPc<sub>2</sub>) overlaps with peak at 680 cm<sup>-1</sup> (weak in Ace-PQ-Ni), and appears at 680 cm<sup>-1</sup> in Ace-PQ-Ni/LuPc<sub>2</sub> heterostructure (medium). However, the strong peak at 1598 cm<sup>-1</sup> consistent with benzene stretching in Ace-PQ-Ni/LuPc<sub>2</sub> heterostructure and the strong peaks at 1408 cm<sup>-1</sup> consistent with isoindole stretching, at 1512 cm<sup>-1</sup> to C=C pyrrole stretching and coupling of pyrrole and aza stretching in AM6/LuPc<sub>2</sub> heterostructure are unique and

can be directly attributed to the LuPc<sub>2</sub> layer<sup>35</sup>. Overall, the spectra of heterostructures are the addition of the spectra of sublayer and top layer.

### Electrical properties of heterojunction devices

Electrical properties of the Ace-PQ-Ni/LuPc<sub>2</sub> and AM6/LuPc<sub>2</sub> bilayer heterojunction devices were investigated by performing I-V measurements in the applied bias range of -10 V to +10 V in dark and under UV light (Fig. 3a and 3b). Both heterojunction devices exhibit symmetric and non-linear behavior in all conditions. Such feature was characteristic of bilayer organic heterojunction devices, originating from of accumulation of mobile charges at the interface<sup>11,36</sup>.

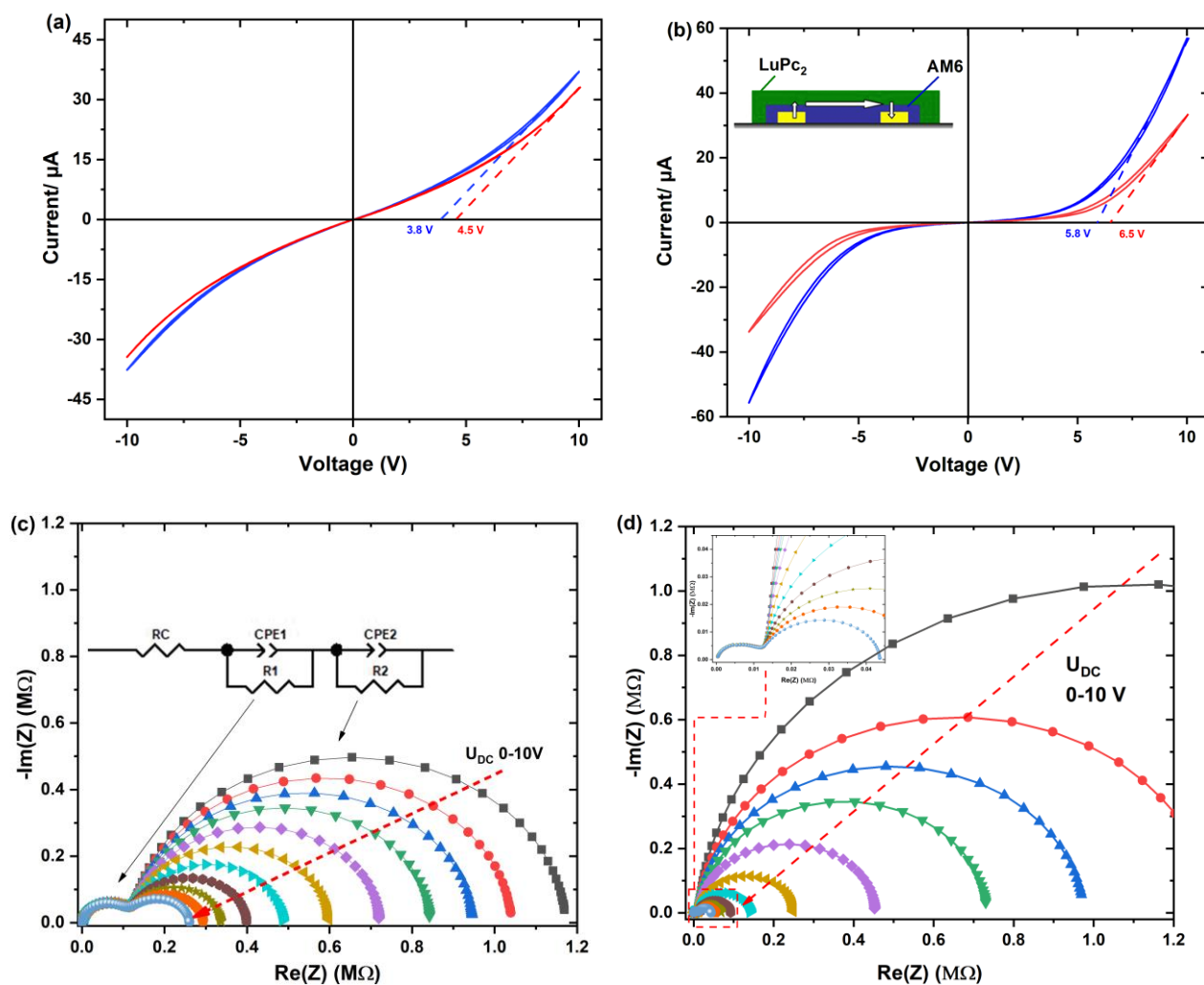


**Figure 3.** I-V characteristics of Ace-PQ-Ni (a) and AM6 (b) based heterojunctions under dark (red curve) and under UV light (blue curve). Inset of Figure (b) represents a simplified device scheme.

Nyquist plots of Ace-PQ-Ni (c) and AM6 (d) based heterojunctions recorded at variable DC voltage

in the range of 0-10 V. The inset of Figure (c) indicates the equivalent circuit selected for fitting Nyquist plots.

Both sublayers are highly resistive compared to LuPc<sub>2</sub><sup>37</sup>. Due to the poor conductive sublayer, the injected charges from electrode experienced high resistance resulting in smaller current at lower voltage. However at higher bias, the injected charges have enough energy to overcome the energy barrier resulting in higher current<sup>11,38</sup>. The non-linearity in I-V curve of heterojunction device is quantified by estimating apparent energy barrier ( $U_{th}$ ) by drawing the tangent at high voltage on the I-V curves and extrapolating it to the X-axis.<sup>10</sup> The apparent energy barrier was calculated for different conditions. The calculated  $U_{th}$  for Ace-PQ-Ni/LuPc<sub>2</sub> and AM6/LuPc<sub>2</sub> in dark was 4.5 V and 6.5 V, respectively. Under light, current increases, as expected for most of the semiconductor-based devices. Thus, current at +10 V was multiplied by 1.13 times for Ace-PQ-Ni/LuPc<sub>2</sub> and by 1.73 times for AM6/LuPc<sub>2</sub> under UV light, with  $U_{th}$  values slightly lower at 3.8 V and 5.8 V, respectively. Whatever the conditions, the energy barrier of AM6/LuPc<sub>2</sub> heterojunction is much higher compared to this of Ace-PQ-Ni/LuPc<sub>2</sub> heterojunction, for both devices.

To further understand the different electrical behaviour of the two heterojunction devices, in depth charge transport studies were performed by impedance spectroscopy in a wide frequency range, from 10 Hz to 10 MHz, at different DC bias. The Nyquist plots of both Ace-PQ-Ni/LuPc<sub>2</sub> and AM6/LuPc<sub>2</sub> heterojunction devices presented two depressed semicircles (Fig. 3c and 3d), in which the one at high frequency (HF, left part) does not change, while the other at low frequency (LF, right part) gets smaller, with increase of DC bias from 0 to 10 V. This confirms the presence of organic-organic interface in the organic heterostructures and the semicircles at HF corresponds to the bulk charge transport, while the semicircles at LF are associated to interfacial charge transport<sup>39</sup>. This can be further validated by the Nyquist plot of a LuPc<sub>2</sub> resistor that exhibits only one depressed semicircle, which size remains independent of the applied DC bias<sup>21</sup>.

To quantitatively determine different charge transport parameters, the experimental Nyquist plots were fitted with constant phase element (CPE) based circuits<sup>40</sup>. CPE is an imperfect capacitor, which impedance is defined by equation (1), where  $Q_i$ ,  $\omega$  and  $\alpha_i$  are non-ideal capacitance, pulsation ( $\omega = 2\pi f$ ,  $f$  being the frequency) and a constant varying between 0 to 1, respectively. CPE turns into a perfect capacitor or a perfect resistor, when  $\alpha$  equals 1 or 0, respectively.

$$Z_{CPE_i}(\omega) = \frac{1}{Q_i \times (j\omega)^{\alpha_i}} \quad (1)$$

The Nyquist plots of both heterojunction devices were modelled by two components  $R_i$ - $CPE_i$  elements connected in series as shown in the inset of Fig. 3c. A contact resistance  $R_c$  is also added in series to take into account the interface between electrode and the sublayer. Here, the  $R_1$ - $CPE_1$  describes the semicircles at HF, while  $R_2$ - $CPE_2$  represents the semicircles at LF, thus they are correlated to bulk and interfacial charge transport, respectively. The fitting resulted in  $R_1$ ,  $\alpha_1$  and  $C_{1\text{eff}}$  as bulk charge transport parameters and  $R_2$ ,  $\alpha_2$  and  $C_{2\text{eff}}$  as interfacial charge transport parameters, which variations with DC bias are depicted in Fig. 4.

$R_1$  value is about ten times lower for AM6-based device than for Ace-PQ-Ni-based device, but  $R_2$  is ca. ten times higher, at 2.2 M $\Omega$  at low bias, which confirms the lower current at low bias. However,  $R_2$  diminishes with bias increase, down to a value comparable for both devices. This explains why at +10 V, current value was higher for AM6-based device compared to Ace-PQ-Ni-based device. For  $\alpha_1$  and  $\alpha_2$ , values are different for both devices, but remain in the same range, namely 0.9 – 1.0, so near 1, which confirms the existence of high capacity at the interfaces for both devices and explains the non-linearity of I-V characteristics. This is also confirmed by the capacitances, in the nF range for  $C_{2\text{eff}}$  and in the pF range for  $C_{1\text{eff}}$ , with values for AM6-based device about twice these of Ace-PQ-Ni-based device.

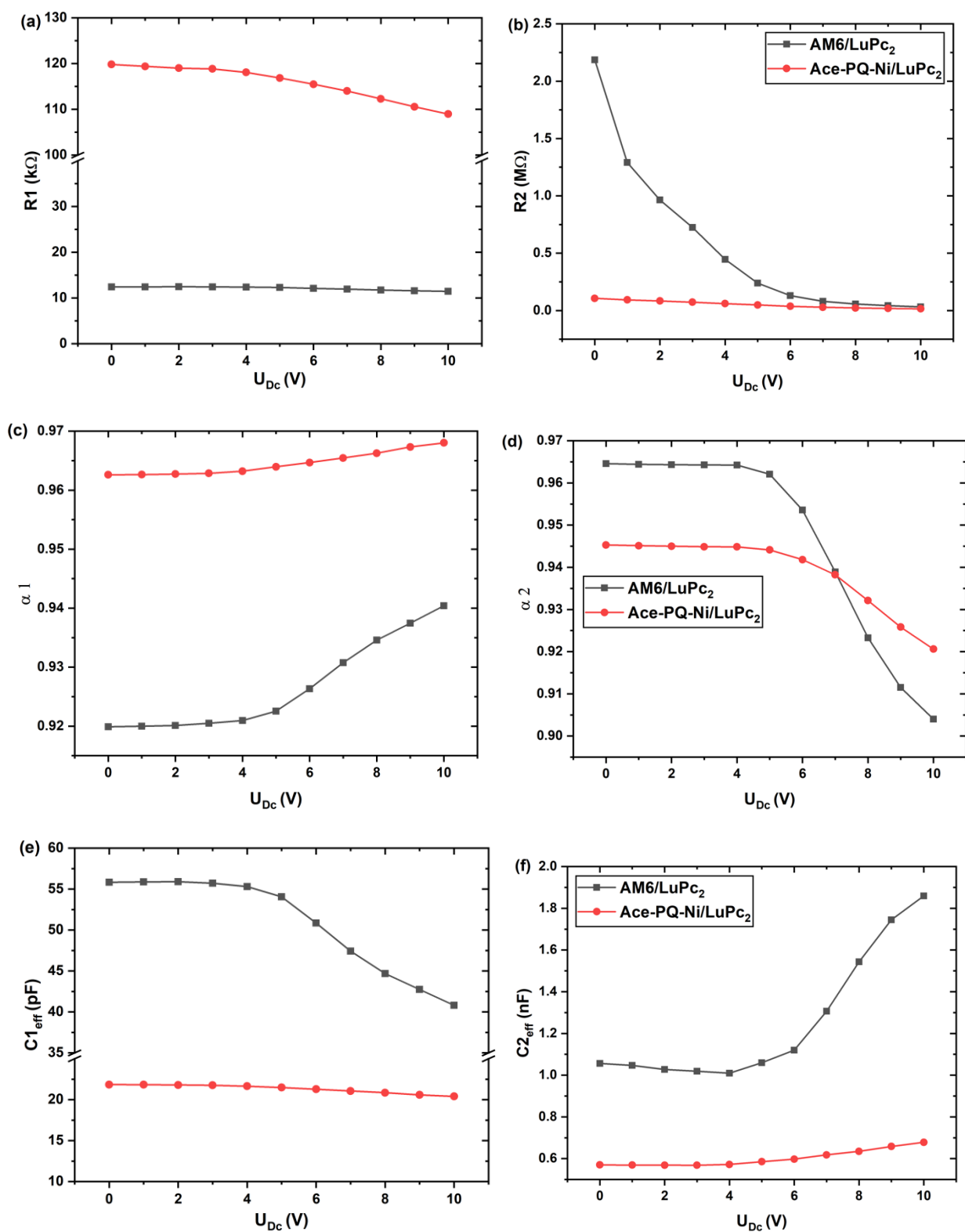


**Figure 4.** Variations of equivalent circuit resistances, R1 (a) and R2 (b),  $\alpha_1$  (c) and  $\alpha_2$  (d), effective capacitances  $C_{1_{eff}}$  (e) and  $C_{2_{eff}}$  (f), as a function of bias (0-10 V) for Ace-PQ-Ni/LuPc<sub>2</sub> and AM6/LuPc<sub>2</sub> heterojunction devices.

### Ammonia sensing properties

Ammonia sensing properties of the heterojunction devices were investigated under high concentration of  $\text{NH}_3$  (90 ppm) for long exposure of 10 min and flow of clean air for 30 min as recovery period. The current variation with time depicted in Fig. 5 (response curve) exhibits a decrease in current under  $\text{NH}_3$  exposure, while an increase of current was observed during the recovery period, which depicts the heterojunction's p-type nature by taking into account the electron donating tendency of ammonia. The electron transfer from  $\text{NH}_3$  molecules to  $\text{LuPc}_2^+$  cations, which are the majority charge carriers in the top layer, leads to a decrease in their density. In turn, this variation in the density of free charge carriers induces a change in the energy barrier at the interface.

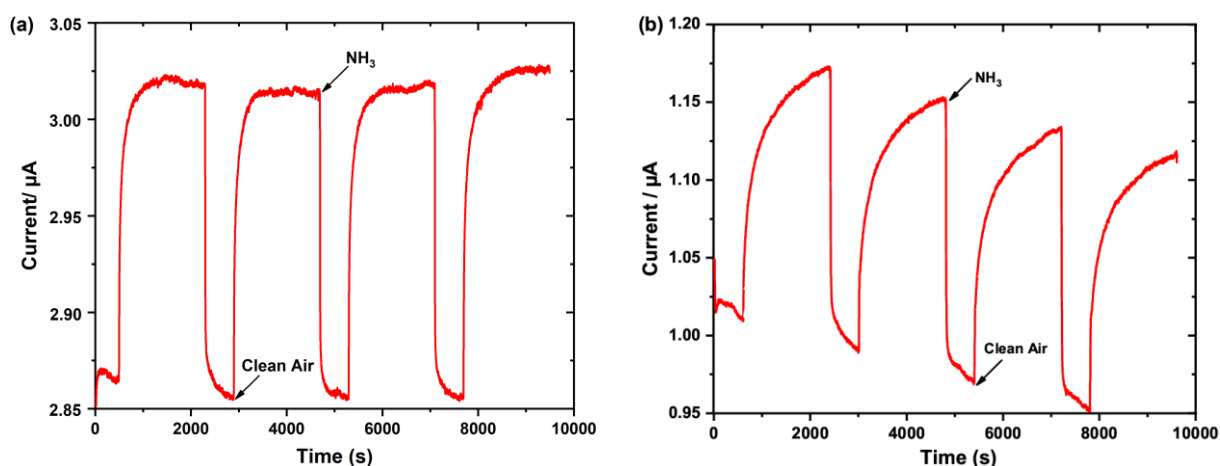


**Figure 5.** Response curve of Ace-PQ-Ni / $\text{LuPc}_2$  (a) and AM6/ $\text{LuPc}_2$  (b) heterojunction sensors, under successive exposures to 90 ppm ammonia for 10 minutes and recovery under clean air for 30 minutes at 45% relative humidity (RH) and room temperature ( $18 - 21^\circ\text{C}$ ).

Notably, Ace-PQ-Ni/ $\text{LuPc}_2$  heterojunction response curve demonstrated very stable baseline with almost complete recovery of the signal during desorption period. On the other hand, AM6/ $\text{LuPc}_2$  shows slight drift in response curve, which mainly attributed to incomplete desorption of the  $\text{NH}_3$  during recovery period. Anyhow, it is worthy to notice that the sensor recovers more

than 85% of its signal during desorption period. A continuous decrease/increase of current was observed throughout exposure/recover cycles for AM6/LuPc<sub>2</sub> heterojunction sensor, while in Ace-PQ-Ni/LuPc<sub>2</sub> heterojunction sensor, a plateau in the response curve was observed during exposure/recovery period. This sorption behaviour of NH<sub>3</sub> in Ace-PQ-Ni/LuPc<sub>2</sub> heterojunction sensor shows that the sorption equilibrium was attained rapidly during exposure/recovery cycles.

Interestingly, different kinetics in response curves of both heterojunction sensors associated with adsorption and desorption rates was evident in response/recovery times. The time taken for both heterojunction sensors to change 90% of its current during exposure period was approximately estimated as 40 sec for Ace-PQ-Ni/LuPc<sub>2</sub> device and twice the same time for AM6/LuPc<sub>2</sub> device. The quick response of both heterojunction sensors towards NH<sub>3</sub> gas were ascribed to the organic heterojunction effect in heterojunction sensors, in which interfacial accumulation of mobile charges facilitates the faster exchange of charges between NH<sub>3</sub> and the sensing layer<sup>41,42</sup>.

To further evaluate the NH<sub>3</sub> sensing properties, both bilayer heterojunction sensors were subjected to short exposure/recovery cycles of 1 min/4 min, under variable NH<sub>3</sub> concentration from 10 to 90 ppm (Fig. 6a and 6b). As quantitative measurement, relative response (RR) of the two sensors was calculated using equation (2), where I<sub>0</sub> and I<sub>f</sub> are initial and final current of an exposure period, respectively. The RR variation as a function of NH<sub>3</sub> concentration of Ace-PQ-Ni/LuPc<sub>2</sub> and AM6/LuPc<sub>2</sub> heterojunction sensors were displayed as calibration curves in Fig. 6c and 6d, respectively.

Both devices show good reproducibility and reversibility that were confirmed by repeating all sets of experiments on a new batch of devices. The uncertainties of the sensors were included as error bar in calibration curves (Fig. 6) and the experimental curves of new batch sensors were shown in Fig. S7.

$$RR(\%) = \frac{I_f - I_0}{I_0} \times 100 \quad (2)$$

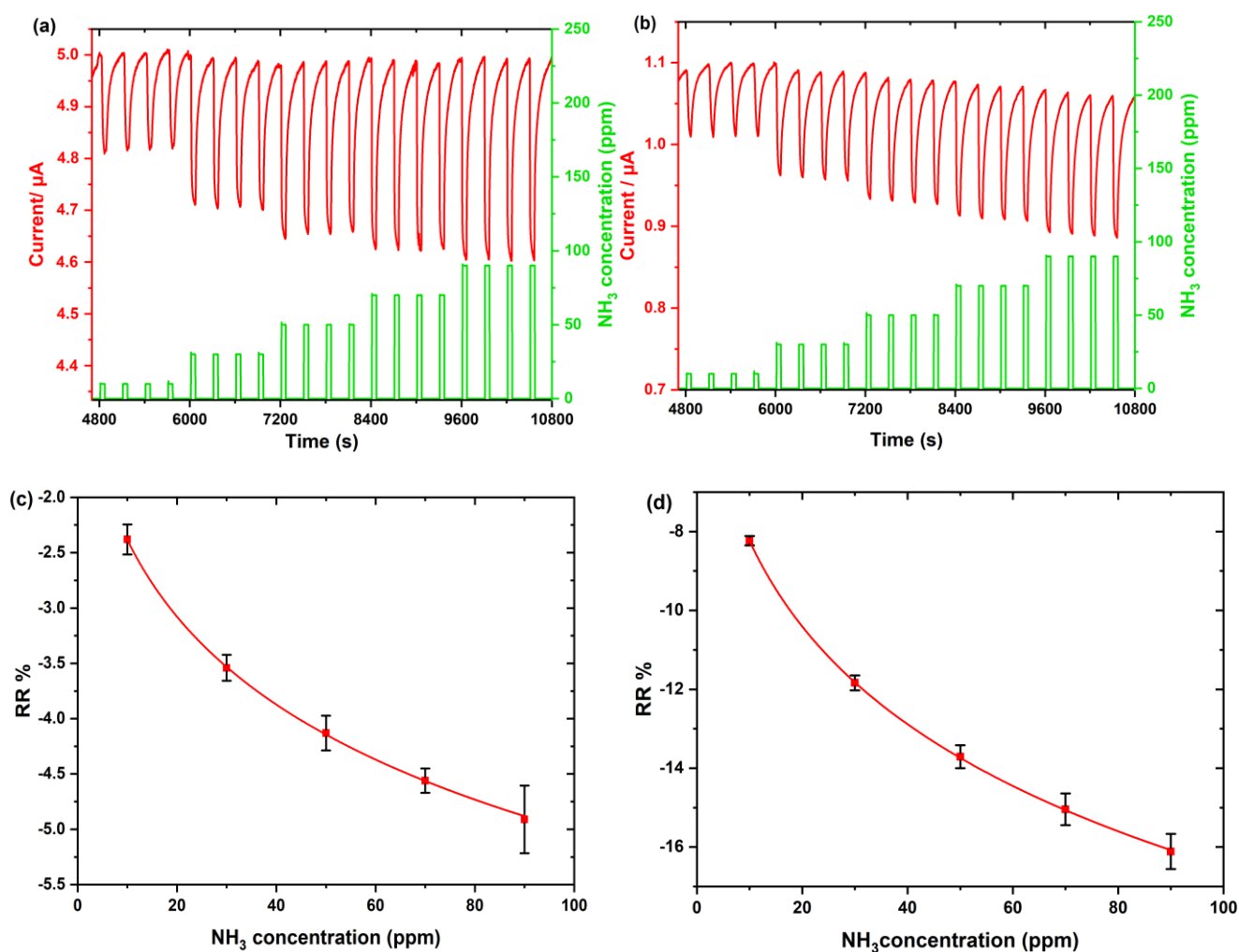


**Figure 6.** Response of Ace-PQ-Ni /LuPc<sub>2</sub> (a) and AM6/LuPc<sub>2</sub> (b) heterojunction sensors under NH<sub>3</sub> gas for 1 min and recovery under clean air for 4 min in the range of NH<sub>3</sub> concentration from 10 to 90 ppm at 45% of RH and room temperature (18–21 °C). The variation of relative response (calibration curve) of Ace-PQ-Ni /LuPc<sub>2</sub> (c) and AM6/LuPc<sub>2</sub> (d) as a function of NH<sub>3</sub> concentration.

RR value of AM6/LuPc<sub>2</sub> based sensor is up to 4 times higher than Ace-PQ-Ni/LuPc<sub>2</sub> sensor as evident from the calibration curve. Notably, the calibration curves are not linear and fit accurately with Langmuir equation. Therefore, the interaction of NH<sub>3</sub> gas molecules on sensor's surface obeys Langmuir type adsorption, in which the number of adsorption sites is limited. At higher concentration, NH<sub>3</sub> gas molecules almost occupied all the available adsorption sites leading to saturation in the sensor signal. Interestingly, both heterojunction sensors exhibit very clear response even at 10 ppm of NH<sub>3</sub> concentration. Hence, both devices were subjected to lower NH<sub>3</sub>

concentration down to 1 ppm (Fig. S8). It is worth mentioning that Ace-PQ-Ni/LuPc<sub>2</sub> and AM6/LuPc<sub>2</sub> based heterojunction sensors can detect NH<sub>3</sub> gas experimentally even at 1 ppm with very low noise.

Limit of detection (LOD) is an important parameter for all chemical gas sensors.<sup>18</sup> LOD was estimated for the heterojunction sensors using equation 3. Here,  $N$  is the noise of the sensor signal,  $S$  is the sensitivity given by the slope of the sensor calibration curve and  $I_0$  is the sensor baseline current.

$$LOD = \frac{3N}{S \cdot I_0} \quad (3)$$

Sensitivity of Ace-PQ-Ni/LuPc<sub>2</sub> heterojunction sensor was determined as  $S = -0.41\% \text{ ppm}^{-1}$  below 5 ppm and  $S = -0.059\% \text{ ppm}^{-1}$  above 5 ppm and for AM6/LuPc<sub>2</sub> heterojunction sensor,  $S = -1.41\% \text{ ppm}^{-1}$  below 5 ppm and  $S = -0.21\% \text{ ppm}^{-1}$  above 10 ppm. Such sensitivity of the sensor led us to obtain a LOD of  $\approx 156$  ppb and 115 ppb for Ace-PQ-Ni/LuPc<sub>2</sub> and AM<sub>6</sub>/LuPc<sub>2</sub> heterojunction sensors, respectively.

The LOD value of both heterojunction sensors is below the daily exposure limit for NH<sub>3</sub> (20 ppm), as suggested by the European Parliament<sup>43</sup>. Additionally, the properties of quick and stable response of both heterojunction sensors even at 1 ppm without huge noise, making it highly suitable for real time applications, even for diseases monitoring application in breath air where concentration of interest are in sub-ppm range<sup>44</sup>.

### **Effect of UV light exposure in ammonia sensing**

Taking into account the light effect on the electrical properties of heterojunction devices, we also carried out sensing experiments under UV light (365 nm) (Fig. 7). As expected for semiconductor-based devices, current increases under light. Surprisingly, both heterojunction sensors show different sensing responses towards NH<sub>3</sub> gas under UV light. Ace-PQ-Ni based heterojunction sensor shows only a weak response to NH<sub>3</sub> under UV light. In addition, we observed a continuous increase in current due to the heating effect of UV light, temperature increasing up to

55 °C, current was finally multiplied by a factor of 2 at the end of light exposure. At this stage, we cannot distinguish between thermal and pure optical effects. On the other hand, with AM6 based heterojunction sensor we observed a greater response to NH<sub>3</sub>, with relative response multiplied by more than 3 at 90 ppm compared to dark, from -10.0% in the dark to -34.33% under light exposure (Fig. 7b, Table 1). This results from a huge increase of  $\Delta I$ , multiplied by more than 13, while current baseline increased by only 3.9. This stronger current increase due to light effect has to be correlated with the higher energy barrier. Under light, the temperature of both samples increased up to 55 °C, while light effect is smaller in sensing response with Ace-PQ-Ni compared to AM6. It should be noted that 365 nm corresponds to a minimum of absorption for both porphyrins (Fig. 2). On the other hand, LuPc<sub>2</sub> is the material that absorbs the most at this wavelength through its Soret band, which confirms that the difference between the two devices is mainly due to the interface between the two layers in each sensor. Actually, upon constant UV illumination, we can distinguish between a short time effect, which is optical in nature, and a slow kinetics effect, which can be attributed to the heating of the device. This thermal effect is visible with Ace-PQ-Ni, but is masked with AM6, due to the high response to NH<sub>3</sub>. In addition, as soon as light is turned off, a sharp decrease is observed, followed by a slow decrease (temperature decrease).

To differentiate the light and temperature effects, both heterojunction sensors were studied under the same concentration of NH<sub>3</sub> gas by increasing the temperature from 20 °C to 55 °C in dark. We observed increasing in current with increasing in temperature, as expected for semiconductor-based devices. For AM6/LuPc<sub>2</sub> sensor, the baseline current was multiplied by 3, but the  $\Delta I$  remain almost the same from 20 °C to 55 °C, leading to a weaker RR. Even though the temperature change shows strong effect in AM6 based heterojunction sensor, it still has nothing to do with increasing in RR under light. It is evident that the unique increase in RR is truly because of light source. Sensitivity of AM6-based heterojunction sensor at 90 ppm NH<sub>3</sub> was increased from -0.21% ppm<sup>-1</sup> in the dark to -0.56% ppm<sup>-1</sup> under light exposure (Fig. 7b, Table 1).

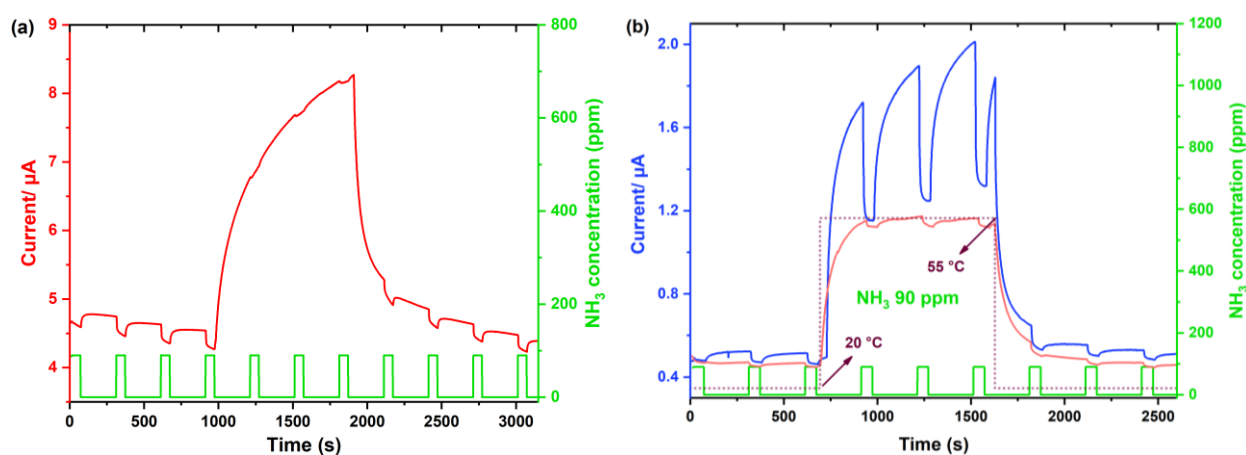


**Figure 7.** Response of Ace-PQ-Ni /LuPc<sub>2</sub> (a) and AM6/LuPc<sub>2</sub> (b) heterojunction sensors under NH<sub>3</sub> concentration of 90 ppm for 1 min/4min exposure/recovery under light exposure (365 nm) at 45% of RH. In (b), current variation was added during the same exposure/recovery cycles, but under a thermal cycle (red line), showing the programmed temperature cycle (dotted line).

To evaluate further, the AM6/LuPc<sub>2</sub> sensor was investigated under a wide range of NH<sub>3</sub> concentration from 10 ppm to 90 ppm under exposure to UV light. Nine cycles were recorded at each given concentration where the light was turned on after third cycle and turned off after sixth cycle, at each concentration, using a homemade software with Arduino UNO board (Fig. 8). At all tested NH<sub>3</sub> concentrations, current increase and decrease under light was reversible, while the sensor response was correlated with the NH<sub>3</sub> concentration. Repeated experiment was shown in Fig. S9 and error bars were given in the calibration curve (Fig. 8b). Under light, the LOD became better than 100 ppb (calc. 83 ppb, Table 1). This value is the best we ever obtained with heterojunction devices. Up to now, 100 ppb had been reported with a silicon phthalocyanine - based heterojunction device and between 100 and 500 ppb in a few examples<sup>36</sup>.

Such response enhancement under light has been already reported, but only with inorganic conductometric gas sensors<sup>45</sup>. Two phenomena can occur in the present molecular material-based sensors. First, light can facilitate dioxygen desorption, increasing the number of available adsorption sites for ammonia molecules. Second, adsorption/desorption processes are generally faster under illumination.

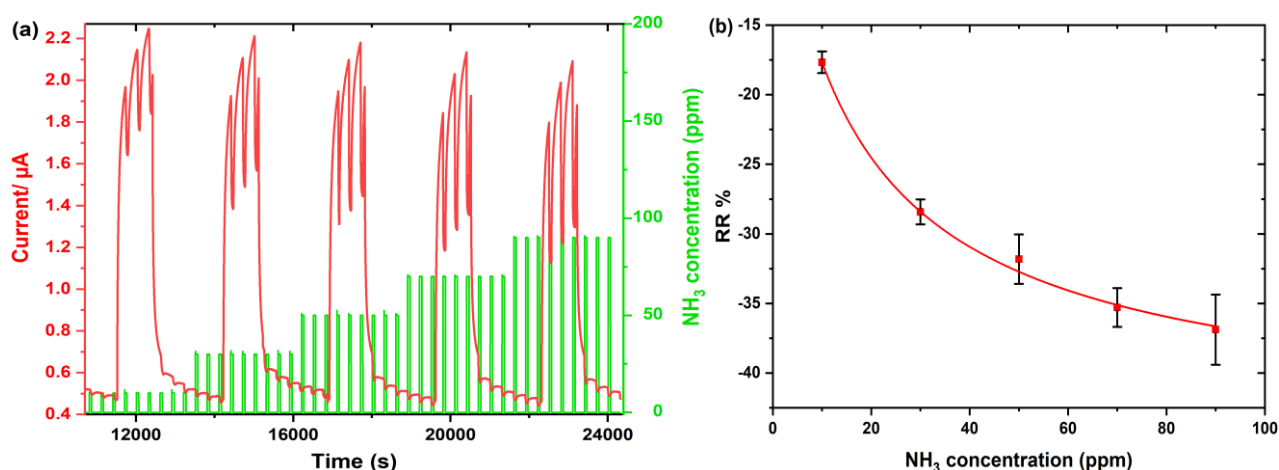


**Figure 8.** (a) Response of AM6/LuPc<sub>2</sub> heterojunction sensors under NH<sub>3</sub> gas for 1 min and recovery under clean air for 4 min in the range of NH<sub>3</sub> concentration from 10 to 90 ppm alternating in the dark and under UV light exposure, at 45% of RH. Calibration curve of AM6/LuPc<sub>2</sub> (b) as a function of NH<sub>3</sub> concentration.

**Table 1.** Comparison of I<sub>0</sub>, ΔI and RR of Ace-PQ-Ni and AM6 based heterojunction sensors in dark and under light, as determined at 90 ppm NH<sub>3</sub> and LOD.

Device	Dark				UV light				Ratio		
									UV light/Dark		
	I <sub>0</sub> (μA)	ΔI (μA)	RR (%)	LOD (ppb)	I <sub>0</sub> (μA)	ΔI (μA)	RR (%)	LOD (ppb)	I <sub>0</sub> (μA)	ΔI (μA)	RR (%)
Ace-PQ-Ni/ LuPc <sub>2</sub>	4.62	-0.27	-5.95	156	-	-	-	-	-	-	-
AM6/ LuPc <sub>2</sub>	0.51	-0.05	-10.0	115	2.01	-0.69	-34.3	83	3.94	13.53	3.40

The difference between the two studied heterojunctions can only come from the nature of the sub-layer. As shown in Fig. 3, AM6/LuPc<sub>2</sub> exhibits a higher energy barrier than Ace-PQ-Ni/LuPc<sub>2</sub> and a stronger light effect. As a result, in sensing experiments, we also observed a higher current increase from dark to light. Current was multiplied by a factor of 4 with AM6 and only 2 with Ace-

PQ-Ni. These results suggest that, under light, a higher density of mobile charges is accumulated in the channel, resulting in a higher sensitivity<sup>41</sup>.

### Humidity effect

When it comes to real-world application, effect of humidity is an important parameter and potential interferent in gas sensing application. Therefore, both heterojunction devices were also investigated under humidity in a broad range, varying monotonically from 30% to 60% then decreasing to initial value as so-called long exposure for 10 min at each RH step. Fig. 9 depicts the current variation of the two sensors at given RH over time.

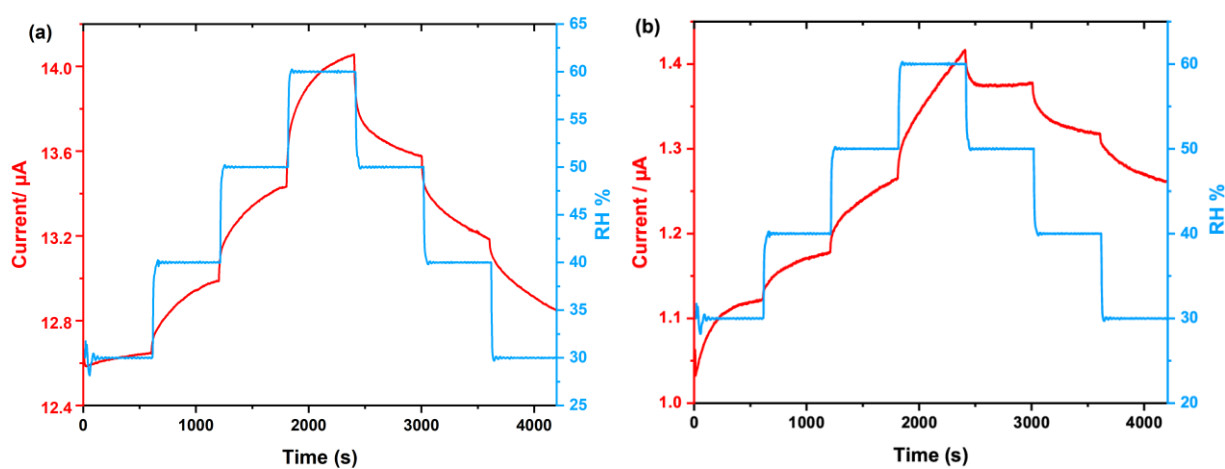


**Figure 9.** Response of Ace-PQ-Ni/LuPc<sub>2</sub> (a) and AM6/LuPc<sub>2</sub> (b) heterojunctions towards the RH change in the range of 30% to 60%, at room temperature (21 °C).

Ace-PQ-Ni/LuPc<sub>2</sub> based sensor shows increase in current during monotonically increase in RH step and decrease during monotonically decrease in RH with good reversibility. On the other hand, AM6/LuPc<sub>2</sub> based sensor reveals a continuous increase in current during steps of RH and exhibits partial recovery during RH decrease, which is attributed to incomplete desorption of the H<sub>2</sub>O molecules during the recovery step, which may get trapped during monotonically increase in RH. Overall, current changes by +27% for AM6/LuPc<sub>2</sub> and only +12 % for Ace-PQ-Ni/LuPc<sub>2</sub>, when RH varies from 30% to 60%, but with a quasi-stabilization of the current after 10 min, compared to -10% for the RR to 90 ppm NH<sub>3</sub> in the dark and -34% under UV light for AM6/LuPc<sub>2</sub>. This difference could be due to morphological differences between the heterojunctions as already

demonstrated with silicon phthalocyanine based gas sensors<sup>36</sup> Here, we observe an opposite response to humidity (current increase) and to NH<sub>3</sub> (current decrease). So, it is difficult to predict the variation of the response to NH<sub>3</sub> upon changing RH value. However, the good point is that the humidity effect is reversible, which is rarely the case, in particular when working at room temperature. So, the combination of our sensors with a humidity sensor could be used to get a corrected value of NH<sub>3</sub> concentration.

The present sensors are not more sensitive to NH<sub>3</sub> than other molecular material-based heterojunctions, but they exhibit a better LOD (Table 2). Clearly, phthalocyanine-based heterojunctions are more sensitive than phthalocyanine-based resistors, exemplified by LuPc<sub>2</sub> resistor<sup>46</sup> and a fluorinated CoPc resistor<sup>47</sup>. Even though double layer heterojunctions are less sensitive than the double lateral heterojunctions<sup>48,49</sup>, they exhibit better LOD, due to a lower noise. Thus, AM6/LuPc<sub>2</sub> exhibits a LOD comparable to the best ever reported for heterojunction devices, i.e. 100 ppb, based on fluorinated silicon phthalocyanine<sup>36</sup> and even better under illumination. It is worth mentioning that the present sensors favorably compete with previously reported devices and operate in humid atmosphere and at room temperature.

About the selectivity, it is known that the response of such conductometric sensors is related to the nature of the target gas. Thus, an oxidizing gas will induce a positive response (since we have p-type devices) and electron-donating species will give a negative response. So, such devices will be first sensitive to strong oxidizing agents like nitrogen dioxide and ozone, then to NH<sub>3</sub>. For other electron-donating species the selectivity will also depend on the strength of the electron-donating character of the target gas.

**Table 2.** Comparison of sensitivities and LODs of Ace-PQ-Ni/LuPc<sub>2</sub> and AM6/LuPc<sub>2</sub> double layer heterojunction devices with other previously reported organic resistors, hybrids and heterojunction devices in dark at room temperature.

Device (Type of charge carriers)	S (% ppm <sup>-1</sup> )	LOD (ppb)	[NH <sub>3</sub> ] (ppm)	Reference
LuPc <sub>2</sub> resistor (p)	-0.02	/	25	46
CoPc[β-O(4-CF <sub>3</sub> -Ph) <sub>4</sub> ] resistor (n)	0.17	420	14-16	47
PEDOT/PSS-SWCNT resistor (p)	-0.21	200	2-100	50
PTFANI/LuPc <sub>2</sub> (p) <sup>a</sup>	-1.05	450	1-10	48
PDMA/LuPc <sub>2</sub> (p) <sup>a</sup>	-1.85	320	1-10	49
pCuTpNH <sub>2</sub> PC/LuPc <sub>2</sub> (n) <sup>a</sup>	0.37	125	1-10	51
(345F) <sub>2</sub> -SiPc/LuPc <sub>2</sub> (p)	-0.6	310	5	36
Cl <sub>2</sub> SiPc/LuPc <sub>2</sub> (p)	-0.13	100	10	36
CuF <sub>16</sub> Pc/LuPc <sub>2</sub> (n)	1.5	280	1-10	52
WO <sub>3</sub> /LuPc <sub>2</sub> (n)	0.2	250	1-10	32
Cu(F <sub>16</sub> Pc)/pNiDPP (n)	-0.403	228	1-50	10
Ace-PQ-Ni/LuPc <sub>2</sub> (p)	-0.059	156	5-10	This work
AM6/LuPc <sub>2</sub> (p)	-0.21 -0.56 <sup>b</sup>	115 83 <sup>b</sup>	5-10	This work

<sup>a</sup>Double lateral heterojunction devices; <sup>b</sup> Under light exposure

## **Conclusion**

Cross-conjugated (Ace-PQ-Ni) and linear-conjugated (AM6)  $\pi$ -extended porphyrins have been introduced to constructing double layer heterojunction devices. Ace-PQ-Ni and AM6 combined with LuPc<sub>2</sub> as an intrinsic semiconductor lead to devices with rather high energy barriers, 4.5 and 6.5 V, respectively, as estimated from I-V characteristics. These values explain the high sensitivity towards NH<sub>3</sub> and the response stability compared to classical resistors, with LOD of 156 and 115 ppb for Ace-PQ-Ni and AM6 – based sensors, respectively. In addition, although both with a current increase, the two porphyrin – based sensors show opposite sensing responses to NH<sub>3</sub> under light illumination. Thus, for Ace-PQ-Ni/LuPc<sub>2</sub> device, the current variation under NH<sub>3</sub> largely decreased upon light illumination. In sharp contrast, the current variation remarkably increased by multiplication factor of 13 for AM6/LuPc<sub>2</sub> sensor under light illumination. This unusual behavior observed for AM6/LuPc<sub>2</sub> sensor can be attributed to the linear conjugation in the  $\pi$ -extended macrocycle of AM6. In comparison, Ace-PQ-Ni is a cross-conjugated  $\pi$ -extended porphyrin. This work paves the way to further studies of  $\pi$ -extended porphyrins in organic electronics devices and gas sensors.

## **Acknowledgments**

The authors acknowledge the Agence Nationale de la Recherche for funding through ANR project PORPH4SENS (ANR-22-CE06-0039-01), the Conseil régional Bourgogne Franche-Comté through the Envergure Program MatElectroCap (2020-2024). S. G. M. acknowledges the Conseil régional Bourgogne Franche-Comté for a Ph. D grant. J. A. and H. W. acknowledge the U.S. Department of Energy, Office of Science, Basic Energy Sciences for financial support under Award DE-SC0016766. The authors thank the Plateforme d'Analyses Chimiques et de Synthèse Moléculaire de l'Université de Bourgogne (PACSMUB) and the SATT Sayens for technical support in the Raman analyses and Prof. Anthony Romieu for the UV light source.

## Supporting Information

The Supporting Information is available free of charges on the ACS Publication website.

Synthesis of fluoranthene-fused tetracenequinone nickel porphyrin (Ace-PQ-Ni),  $^1\text{H}$  and  $^{13}\text{C}$  NMR spectra, scheme of the quasi-dip coating method, Raman data, response to  $\text{NH}_3$  of a second batch of Ace-PQ-Ni/LuPc<sub>2</sub> and AM6/LuPc<sub>2</sub> devices and responses at low  $\text{NH}_3$  concentrations.

## References

- (1) Rakow, N. A.; Suslick, K. S. A Colorimetric Sensor Array for Odour Visualization. *Nature* **2000**, *406* (6797), 710–713.
- (2) Di Natale, C.; Filippini, D.; Pennazza, G.; Santonico, M.; Paolesse, R.; Bellincontro, A.; Mencarelli, F.; D'Amico, A.; Lundström, I. Sorting of Apricots with Computer Screen Photoassisted Spectral Reflectance Analysis and Electronic Nose. *Sens. Actuators: B. Chem.* **2006**, *119* (1), 70–77.
- (3) Paolesse, R.; Monti, D.; La Monica, L.; Venanzi, M.; Froiio, A.; Nardis, S.; Di Natale, C.; Martinelli, E.; D'Amico, A. Preparation and Self-Assembly of Chiral Porphyrin Diads on the Gold Electrodes of Quartz Crystal Microbalances: a Novel Potential Approach to the Development of Enantioselective Chemical Sensors. *Chem. Eur. J.* **2002**, *8* (11), 2476–2483.
- (4) Macagnano, A.; Sgreccia, E.; Zampetti, E.; Pantalei, S.; Di Natale, C.; Paolesse, R.; D'Amico, A. Potentials and Limitations of a Porphyrin-Based at-Cut Resonator for Sensing Applications. *Sens. Actuators: B. Chem.* **2008**, *130*, 411–417.
- (5) Garg, K.; Singh, A.; Debnath, A. K.; Nayak, S. K.; Chattopadhyay, S.; Aswal, D. K.; Hayakawa, Y.; Gupta, S. K.; Yakhmi, J. V. Bis-Porphyrin Films as Ppb Level Chemiresistive Sensors. *Chem. Phys. Lett.* **2010**, *488*, 27–31.
- (6) Penza, M.; Rossi, R.; Alvisi, M.; Signore, M. A.; Serra, E.; Paolesse, R.; Amico, A. D.; Di Natale, C. Metalloporphyrins-Modified Carbon Nanotubes Networked Films-Based Chemical Sensors for Enhanced Gas Sensitivity. *Sens. Actuators: B. Chem.* **2010**, *144* (2), 387–394.
- (7) Saxena, S.; Verma, A. L. Metal-Tetraphenylporphyrin Functionalized Carbon Nanotube Composites as Sensor for Benzene, Toluene and Xylene Vapors. *Adv. Mater. Res.* **2014**, *5* (8), 472–478.
- (8) Liu, S. S.; Moh, L. C. H.; Swager, T. M. Single-Walled Carbon Nanotube–Metalloporphyrin Chemiresistive Gas Sensor Arrays for Volatile Organic Compounds. *Chem. Mater.* **2015**, *27*, 3560–3563.
- (9) Kumar, A.; Alami Mejjati, N.; Meunier-Prest, R.; Krystianiak, A.; Heintz, O.; Lesniewska, E.; Devillers, C. H.; Bouvet, M. Tuning of Interfacial Charge Transport in Polyporphine/Phthalocyanine Heterojunctions by Molecular Geometry Control for an Efficient Gas Sensor. *Chem. Eng. J.* **2022**, *429*, 132453.
- (10) Bengasi, G.; Meunier-Prest, R.; Baba, K.; Kumar, A.; Pellegrino, A. L.; Boscher, N. D.; Bouvet, M. Molecular Engineering of Porphyrin-Tapes/Phthalocyanine Heterojunctions for a Highly Sensitive Ammonia Sensor. *Adv. Electron. Mater.* **2020**, *6* (12), 2000812.
- (11) Wang, H.; Yan, D. Organic Heterostructures in Organic Field-Effect Transistors. *NPG Asia Mater.* **2010**, *2* (2), 69–78.
- (12) Bouvet, M.; Gaudillat, P.; Kumar, A.; Sauerwald, T.; Schüler, M.; Schütze, A.; Suisse, J.-M. Revisiting the Electronic Properties of Molecular Semiconductor – Doped Insulator (MSDI) Heterojunctions Through Impedance and Chemosensing Studies. *Org. Electron.* **2015**, *26*, 345–354.

- (13) Comini, E.; Cristalli, A.; Faglia, G.; Sberveglieri, G. Light Enhanced Gas Sensing Properties of Indium Oxide and Tin Dioxide Sensors. *Sens. Actuators: B. Chem.* **2000**, *65* (1-3), 260–263.
- (14) Comini, E.; Faglia, G.; Sberveglieri, G. UV Light Activation of Tin Oxide Thin Films for NO<sub>2</sub> Sensing at Low Temperatures. *Sens. Actuators: B. Chem.* **2001**, *78* (1-3), 73–77.
- (15) Gonzalez, O.; Welearegay, T. G.; Vilanova, X.; Llobet, E. Using the Transient Response of WO<sub>3</sub> Nanoneedles Under Pulsed UV Light in the Detection of NH<sub>3</sub> and NO<sub>2</sub>. *Sensors* **2018**, *18* (5), 1346.
- (16) Nakamura, Y.; Ishikura, Y.; Morita, Y.; Takagi, H.; Fujitsu, S. Photo-Assisted Aromatic VOC Sensing by a P-NiO:Li/N-ZnO Transparent Heterojunction Sensor Element. *Sens. Actuators: B. Chem.* **2013**, *187*, 578–585.
- (17) Chen, H.; Zhang, M.; Bo, R.; Barugkin, C.; Zheng, J.; Ma, Q.; Huang, S.; Ho-Baillie, A. W. Y.; Catchpole, K. R.; Tricoli, A. Superior Self-Powered Room-Temperature Chemical Sensing with Light-Activated Inorganic Halides Perovskites. *Eur. J. Inorg. Chem.* **2018**, *14* (7), 1702571.
- (18) Sivalingam, Y.; Martinelli, E.; Catini, A.; Magna, G.; Pomarico, G.; Basoli, F.; Paolesse, R.; Di Natale, C. Gas-Sensitive Photoconductivity of Porphyrin-Functionalized ZnO Nanorods. *J. Phys. Chem. C* **2012**, *116* (16), 9151–9157.
- (19) Magna, G.; Muduganti, M.; Stefanelli, M.; Sivalingam, Y.; Zurlo, F.; Di Bartolomeo, E.; Catini, A.; Martinelli, E.; Paolesse, R.; Di Natale, C. Light-Activated Porphyrinoid-Capped Nanoparticles for Gas Sensing. *ACS Appl. Nanomat.* **2021**, *4* (1), 414–424.
- (20) Alzate-Carvajal, N.; Park, J.; Pykal, M.; Lazar, P.; Rautela, R.; Scarfe, S.; Scarfe, L.; Ménard, J.-M.; Otyepka, M.; Luican-Mayer, A. Graphene Field Effect Transistors: a Sensitive Platform for Detecting Sarin. *ACS Appl. Mater. Interfaces* **2021**, *13* (51), 61751–61757.
- (21) Loma Kikobo, G.; Kumar, A.; Vibhu, V.; Ouedraogo, S.; Deshotel, A.; Mateos, M.; Meunier-Prest, R.; Bouvet, M. Photon Assisted-Inversion of Majority Charge Carriers in Molecular Semiconductor-Based Organic Heterojunctions. *J. Mater. Chem. C* **2021**, *9*, 5008–5020.
- (22) Turek, P.; Petit, P.; André, J.-J.; Simon, J.; Even, R.; Boudjema, B.; Guillaud, G.; Maitrot, M. A New Series of Molecular Semiconductors: Phthalocyanine Radicals. *J. Am. Chem. Soc.* **1987**, *109* (17), 5119–5122.
- (23) Bouvet, M. Radical Phthalocyanines and Intrinsic Semiconduction. In *The Porphyrin Handbook*; Kadish, K. M., Smith, K. M., Guillard, R., Eds.; Academic Press, 2003; Vol. 19, pp 37–103.
- (24) Parra, V.; Brunet, J.; Pauly, A.; Bouvet, M. Molecular Semiconductor-Doped Insulator (MSDI) Heterojunctions: an Alternative Transducer for Gas Chemosensing. *Analyst* **2009**, *134* (9), 1776–1778.
- (25) Carvalho, C. M.; Brocksom, T. J.; de Oliveira, K. T. Tetrabenzoporphyrins; Synthetic Developments and Applications. *Chem. Soc. Rev.* **2013**, *42* (8), 3302–3317.
- (26) Roznyatovskiy, V. V.; Lee, C.-H.; Sessler, J. L.  $\Pi$ -Extended Isomeric and Expanded Porphyrins. *Chem. Soc. Rev.* **2013**, *42* (5), 1921–1933.
- (27) Moss, A.; Nevenon, D. E.; Hu, Y.; Nesterov, V. N.; Nemykin, V. N.; Wang, H. Unsymmetric Pentacene- and Pentacenequinone-Fused Porphyrins: Understanding the Effect of Cross- and Linear-Conjugation. *ACS Phys Chem Au* **2022**, *2* (6), 468–481.
- (28) Jiang, L.; Zaenglein, R. A.; Engle, J. T.; Mittal, C.; Hartley, C. S.; Ziegler, C. J.; Wang, H. Pentacene-Fused Diporphyrins. *Chem. Eur. J.* **2014**, *20*, 13865–13870.
- (29) Hu, Y.; Thomas, M. B.; Webre, W. A.; Moss, A.; Jinadasa, R. G. W.; Nesterov, V. N.; D'Souza, F.; Wang, H. Nickel(II) Bisporphyrin-Fused Pentacenes Exhibiting Abnormal High Stability. *Angew. Chem. Int. Ed. Engl.* **2020**, *59* (45), 20075–20082.
- (30) Clarisse, C.; Riou, M. T. Synthesis and Characterization of Some Lanthanide Phthalocyanines. *Inorg. Chim. Acta* **1987**, *130* (1), 139–144.

- (31) Di Zazzo, L.; Ganesh Moorthy, S.; Meunier-Prest, R.; Lesniewska, E.; Di Natale, C.; Paolesse, R.; Bouvet, M. Ammonia and Humidity Sensing by Phthalocyanine-Corrole Complex Heterojunction Devices. *Sensors* **2023**, *23*, 6773.
- (32) Bouvet, M.; Mateos, M.; Wannebroucq, A.; Navarrete, E.; Llobet, E. Tungsten Oxide – Lutetium Bisphthalocyanine N-P-N Hetero-Junction: From Nanomaterials to a New Transducer for Chemo-Sensing. *J. Mater. Chem. C* **2019**, *7*, 6448–6455.
- (33) Even, R.; Simon, J.; Markovitsi, D. Optical Properties of Thin Films of Molecular Semiconductors. *Chem. Phys. Lett.* **1989**, *156* (6), 609–614.
- (34) Orti, E.; Brédas, J. L.; Clarisse, C. Electronic Structure of Phthalocyanines: Theoretical Investigation of the Optical Properties of Phthalocyanine Monomers, Dimers, and Crystals. *J. Chem. Phys.* **1990**, *92* (2), 1228–1235.
- (35) Ouedraogo, S.; Coulibaly, T.; Meunier-Prest, R.; Bayo-Bangoura, M.; Bouvet, M. p-Type and n-Type Conductometric Behaviors of Octachloro-Metallophthalocyanine-Based Heterojunctions, the Key Role of the Metal. *J. Porphyrins Phthalocyanines* **2020**, *24*, 750–757.
- (36) Ganesh Moorthy, S.; King, B.; Kumar, A.; Lesniewska, E.; Lessard, B. H.; Bouvet, M. Molecular Engineering of Silicon Phthalocyanine to Improve the Charge Transport and Ammonia Sensing Properties of Organic Heterojunction Gas Sensors. *Adv. Sens. Res.* **2022**, 2200030.
- (37) André, J.-J.; Holczer, K.; Petit, P.; Riou, M.-T.; Clarisse, C.; Even, R.; Fourmigué, M.; Simon, J. Electrical and Magnetic Properties of Thin Films and Single Crystals of Bis(Phthalocyaninato)Lutetium. *Chem. Phys. Lett.* **1985**, *115* (4-5), 463–466.
- (38) Kumar, A.; Meunier-Prest, R.; Lesniewska, E.; Bouvet, M. Interplay of Electrode Geometry and Bias on Charge Transport in Organic Heterojunction Gas Sensors. *Sens. Actuators: B. Chem.* **2022**, *369*, 132313.
- (39) Miller, K. A.; Yang, R. D.; Hale, M. J.; Park, J.; Fruhberger, B.; Colesniuc, C. N.; Schuller, I. K.; Kummel, A. C.; Trogler, W. C. Electrode Independent Chemoresistive Response for Cobalt Phthalocyanine in the Space Charge Limited Conductivity Regime. *J. Phys. Chem. B* **2006**, *110* (1), 361–366.
- (40) Hirschorn, B.; Orazem, M. E.; Tribollet, B.; Vivier, V.; Frateur, I.; Musiani, M. Determination of Effective Capacitance and Film Thickness From Constant-Phase-Element Parameters. *Electrochim. Acta* **2010**, *55* (21), 6218–6227.
- (41) Kumar, A.; Meunier-Prest, R.; Herbst, F.; Heintz, O.; Lesniewska, E.; Bouvet, M. Covalent Grafting of Aryls to Modulate the Electrical Properties of Phthalocyanine-Based Heterostructures: Application to Ammonia Sensing. *Chem. Eng. J.* **2022**, *436*, 135207.
- (42) Ouedraogo, S.; Meunier-Prest, R.; Kumar, A.; Bayo-Bangoura, M.; Bouvet, M. Modulating the Electrical Properties of Organic Heterojunction Devices Based on Phthalocyanines for Ambipolar Sensors. *ACS Sens.* **2020**, *5* (6), 1849–1857.
- (43) *Directive 2008/50/EC of the European Parliament and of the Council of 21 May 2008, on Ambient Air Quality and Cleaner Air for Europe*; 2008; Vol. L 152, pp 1–44.
- (44) Di Natale, C.; Paolesse, R.; Martinelli, E.; Capuano, R. Solid-State Gas Sensors for Breath Analysis: a Review. *Anal. Chim. Acta* **2014**, *824*, 1–17.
- (45) Kumar, R.; Liu, X.; Zhang, J.; Kumar, M. Room-Temperature Gas Sensors Under Photoactivation: From Metal Oxides to 2D Materials. *Nanomicro Lett* **2020**, *12* (1), 164–37.
- (46) Bouvet, M.; Gaudillat, P.; Suisse, J.-M. Lanthanide Macrocyclic Complexes: From Molecules to Materials and From Materials to Devices. *J. Porphyrins Phthalocyanines* **2013**, *17*, 628–635.
- (47) Duan, X.; Zhang, Y.; Wang, H.; Dai, F.; Yang, G.; Chen, Y. A Phthalocyanine Sensor Array Based on Sensitivity and Current Changes for Highly Sensitive Identification of Three Toxic Gases at Ppb Levels. *New J. Chem.* **2020**, *44* (31), 13240–13248.
- (48) Mateos, M.; Meunier-Prest, R.; Heintz, O.; Herbst, F.; Suisse, J.-M.; Bouvet, M. Comprehensive Study of Poly(2,3,5,6-Tetrafluoroaniline): From Electrosynthesis to

Heterojunctions and Ammonia Sensing. *ACS Appl. Mater. Interfaces* **2018**, 10 (23), 19974–19986.

- (49) Mateos, M.; Tchangäi, M.-D.; Meunier-Prest, R.; Heintz, O.; Herbst, F.; Suisse, J.-M.; Bouvet, M. Low Conductive Electrodeposited Poly(2,5-Dimethoxyaniline) as a Key Material in a Double Lateral Heterojunction, for Sub-Ppm Ammonia Sensing in Humid Atmosphere. *ACS Sens.* **2019**, 4 (3), 740–747.
- (50) Jian, J.; Guo, X.; Lin, L.; Cai, Q.; Cheng, J.; Li, J. Gas-Sensing Characteristics of Dielectrophoretically Assembled Composite Film of Oxygen Plasma-Treated SWCNTs and PEDOT/PSS Polymer. *Sens. Actuators: B. Chem.* **2013**, 178, 279–288.
- (51) Di Zazzo, L.; Kumar, A.; Meunier-Prest, R.; Di Natale, C.; Paolesse, R.; Bouvet, M. Electrosynthesized Copper Polycorroles as Versatile Materials in Double Lateral Heterojunctions. *Chem. Eng. J.* **2023**, 458, 141465.
- (52) Mateos, M.; Meunier-Prest, R.; Suisse, J.-M.; Bouvet, M. Modulation of the Organic Heterojunction Behavior, From Electrografting to Enhanced Sensing Properties. *Sens. Actuators: B. Chem.* **2019**, 299, 126968.